Nuclear Inst. and Methods in Physics Research, A 953 (2020) 163267

Contents lists available at ScienceDirect

Nuclear Inst. and Methods in Physics Research, A

journal homepage: www.elsevier.com/locate/nima

Production and characterization of thin, self-supporting Si foils for use as targets in radioactive beam experiments

J.E. Johnstone [a,b], S. Hudan [a,b], C. Folluo [a], T. Werke [a,b,1], P.A. DeYoung [c], R.T. deSouza [a,b,*]

[a] Department of Chemistry, Indiana University, 800 E. Kirkwood Ave., Bloomington, IN 47405, USA
[b] Center for Exploration of Energy and Matter, Indiana University, 2401 Milo B. Sampson Lane, Bloomington, IN 47408, USA
[c] Physics Department, VanderWerf Hall, 27 Graves Place, Holland, MI 49423, USA

ARTICLE INFO

Keywords:
Silicon foils
Target thickness determination
Target purity
Self-supporting foils
Vapor deposition

ABSTRACT

Development of thin, self-supporting silicon foils (both natural and isotopically-enriched) for use as targets in reaction studies with radioactive beams is detailed. Foils with a thickness of ~220 μg/cm^2 were produced using vapor deposition and were floated onto aluminum frames with 10–15 mm diameter holes. During their production, the foil thickness was measured using a quartz crystal monitor. Subsequently, the foil thickness was characterized by α particle energy loss measurements and Rutherford backscattering (RBS). These measurements demonstrated that the thickness could be determined to within a 0.5% uncertainty. The elemental purity of the foils was assessed using RBS and X-ray photoelectron spectroscopy. This analysis demonstrated that the foils have 87%–90% silicon abundance.

1. Introduction

Nuclear reactions of neutron-rich nuclei is a topic of considerable interest for the fields of both nuclear physics and nuclear astrophysics [1]. Recent measurements of the near-barrier fusion excitation function for ^{39,47}K + ^{28}Si reveal a 7-fold increase in the relative fusion cross-section of the neutron-rich isotope relative to the stable isotope at energies just below the barrier [2]. A key element in these fusion studies with radioactive beams is the production and characterization of high-quality target foils that are both elementally and isotopically pure. Knowledge of the target thickness, as well as assessment of any contaminants, is important for the extraction of the fusion cross-section. Contaminants in the target, particularly those with a slightly lower atomic number present a significant source of background in the measurement of the fusion cross-section. The presence of such a contaminant makes it necessary to distinguish products from fusion of the beam with the lighter contaminant from products associated with the reaction of interest. For silicon targets, oxygen is often a troublesome contaminant. In a prior experiment [2], the silicon targets used exhibited a significant oxygen content (~40%). Though resolvable, the products from K + O presented an unnecessary background introducing an additional source of uncertainty in the measured fusion cross-section. To address this problem, we elected to develop an electron-beam (e-beam) vapor deposition system to enable the fabrication of high-quality targets of refractory materials at Indiana University.

Several techniques for the production of silicon targets have been previously used [3,4]. To produce silicon foils with minimal oxygen contamination the vapor deposition approach [3] was employed. Following construction of an e-beam vapor deposition system, the device was commissioned and the evaporation procedure was optimized using ^{nat}Si. Subsequently, isotopically-enriched ^{28}Si foils were produced. To characterize the foils produced, several measurements were performed. Foil thickness was determined by using α particle energy loss measurements through the foils (α gauge), as well as Rutherford backscattering (RBS) measurements. In order to assess the elemental purity of the foils, both RBS and X-ray photoelectron spectroscopy (XPS) were utilized. Characterization of the foils using the above techniques showed them to consist of 87%–90% silicon with an effective thickness of ~ 220 μg/cm^2. Details of the e-beam vapor deposition system constructed, its use in producing silicon targets, and the characterization of the targets produced are presented below.

2. Electron beam source and vacuum chamber

The e-beam vapor deposition system constructed uses the Ferrotec/Temescal Model 1CK Convertible Electron Beam Turret Source as its central element. This e-beam source is capable of providing a beam of up to 10 keV electrons with an emission current up to 1.5 A (10 kW maximum). For all evaporations described in this manuscript the filament was operated at a maximum current setting of 300 mA. The electron beam produced by the filament is accelerated and deflected by

* Corresponding author at: Department of Chemistry, Indiana University, 800 E. Kirkwood Ave., Bloomington, IN 47405, USA.
E-mail address: desouza@indiana.edu (R.T. deSouza).
[1] Present address: Department of the Army, Rock Island Arsenal, Rock Island, Illinois 61299, USA.

https://doi.org/10.1016/j.nima.2019.163267
Received 1 November 2019; Received in revised form 2 December 2019; Accepted 8 December 2019
Available online 11 December 2019
0168-9002/

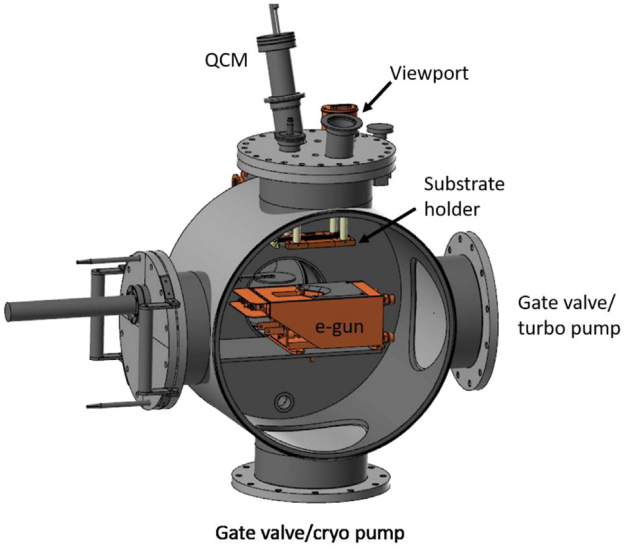

Fig. 1. CAD drawing of the chamber housing the vapor deposition system. The large side flange used as the main access to the chamber is omitted.

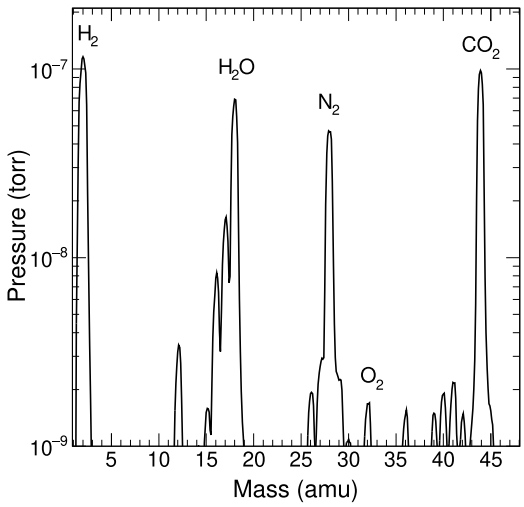

Fig. 2. Mass spectrum from the residual gas in the evaporation chamber following bake-out measured by the RGA.

270° before striking the sample placed in a copper crucible. To separate the evaporant from the copper crucible a liner of either molybdenum or tantalum is typically used. The crucible has 4 pockets which allows vapor deposition of up to four materials without venting the vacuum chamber. Additionally, the electron beam source has the ability to sweep the electron beam in two dimensions in order to provide even heating of the material in the crucible liner. The copper crucible is water cooled using a Haskris WW2 water chiller [5] which allows circulation of 20 °C water at a rate of 2.75 gpm.

Successful production of silicon foils with reduced oxygen content requires achieving a good vacuum ($P \sim 10^{-7}$ torr) in the evaporation chamber prior to commencing the evaporation. In order to accomplish this, a stainless steel chamber was re-purposed to house the electron beam evaporation assembly as shown in Fig. 1. Moreover, to provide a clean environment and facilitate attainment of a good vaccum, the chamber was electropolished. The chamber is pumped using an Edwards STP-603 turbomolecular pump (650 l/s N_2) backed by a Edwards nXDS15i scroll pump to maintain an oil-free environment [6]. Following evacuation to $P < 5 \times 10^{-5}$ torr, a CTI-8 cryopump (1500 l/s air) is used to further reduce the chamber pressure [7]. During evaporation, to protect the turbopump from evaporated material, the gate valve at its entrance is closed and pumping is maintained using only the cryopump. The optimal base vacuum of the chamber is achieved by using a bake-out procedure which involved heating the chamber up to 130 °C at vacuum for up to 72 h. With baking, a pressure of 1.5×10^{-7} torr is attained. The residual gas in the chamber following bake-out was assessed using a Stanford Research Systems RGA 200 [8]. The spectrum from the RGA is presented in Fig. 2. The majority of the gas remaining in the chamber is hydrogen, carbon dioxide, water vapor, and nitrogen. The small peak at mass = 32 corresponds to oxygen and represents a partial pressure of approximately 1×10^{-9} torr. Based upon the chamber total pressure, this corresponds to approximately 1% oxygen content in the residual chamber gas.

The electron gun is mounted on an ISO200 flange facilitating its removal from the chamber if necessary. Mounted on the same flange as the electron gun is a stainless steel shutter. This shutter prevents deposition of evaporated material from the crucible during initial heating of the material. The shutter is operated from outside the chamber by manipulating a linear-motion vacuum feedthrough (Huntington L-2212-6) [9]. Access to the interior of the chamber is provided through the large side flange. This access is essential to mount and dismount the target substrate, clean the inside of the chamber, and resupply material to the crucible after each evaporation. The top flange provides a viewport through which the motion of the electron beam in the crucible pocket can be observed during evaporation. It also provides feedthroughs for a quartz crystal monitor (QCM Model 851) [10] used for monitoring the deposition rate during evaporation and for heating and monitoring the temperature of the copper substrate holder.

Heating of the substrate during evaporation allows relaxation of stress in the deposited material. The evaporation system is therefore designed to allow for the heating of the substrate. The substrate holder is suspended from the top flange of the chamber with ceramic stand-offs to provide electrical and thermal isolation between the heating block and the chamber. This substrate holder is a copper block with 3.2 mm (1/8 in.) diameter cylindrical channels. Ceramic tubes placed in these channels provided electrical isolation for the tantalum wire (99.9%) [11] which serves as the resistive heating element. The 33 cm of Ta wire (0.25 mm diameter) has a resistance of 5 Ω. Application of a voltage of 16 V across the wire by a Tekpower TP3005P Programmable Power Supply results in a current that heats the copper block. The temperature of the substrate holder is monitored using a thermocouple. Substrates are mechanically attached to the substrate holder using 2 copper straps which screw into the block.

3. Silicon foil production

Substrate preparation. Two different substrates were used to produce silicon foils. Initial attempts used tungsten substrates as tungsten had been reported as optimal for the production of silicon targets [3]. Selection of tungsten as a substrate was justified by the close match of its coefficient of linear expansion (4.5 μm $°C^{-1}$) as compared to that of silicon (3.0 μm $°C^{-1}$) [12]. The tungsten substrates used were 25 mm × 75 mm in area and 0.23 mm thick. Prior to their use, to reduce surface roughness the tungsten substrates were electropolished. Parameters for electropolishing the tungsten substrates were adjusted from parameters used in electropolishing tungsten STM probes [13]. Tungsten substrates were submerged in a 0.25 M NaOH solution and electropolished for 5 min at a current density of 13.5 A/dm^2. Two 50 mm × 100 mm stainless steel plates placed on either side of the substrate served as cathodes. After electropolishing, the substrates were cleaned using an Alconox detergent bath and subsequently rinsed with de-ionized water.

Following initial work with tungsten substrates, the use of copper substrates was investigated. Copper had also been reported in the literature as a successful substrate for production of silicon foils [4]. The

copper substrates used were the same area as the tungsten substrates with a thickness of 0.30 mm. Prior to evaporation, the copper substrates were electropolished following well-established procedures [14]. The electropolishing solution consisted of a well-mixed, aqueous solution of 50% phosphoric acid (H_3PO_4). Optimal electropolishing results were achieved by not stirring the solution during electropolishing. The copper substrates were electropolished for 15 min using a current density of 15 A/dm^2 and subsequently cleaned in the same manner as the tungsten substrates.

^{nat}Si foil production. Prior to evaporation, the evaporation chamber was first evacuated to a pressure lower than 5×10^{-7} torr and the copper substrate holder was heated to a temperature of 360 °C. The Telemark 851 Quartz Crystal Monitor provided a measure of the deposition of material during evaporation.

The first step in preparing the substrate for deposition of silicon was the deposition of a release agent. Barium chloride ($BaCl_2$) with greater than 99% purity was used for this purpose. The $BaCl_2$ was first formed from a powder into 200 mg pellets using a DAKE 10,000 psi manual hydraulic press held at 1000 psi of pressure for 20 s. Prior to loading, the $BaCl_2$ pellets were baked using a hot plate to reduce their water content. For each evaporation, a total of 12 pellets (2.4 g) of $BaCl_2$ were deposited into a molybdenum crucible liner and placed into one of the crucible pockets. To reduce the oxygen in the residual gas, titanium was used as an oxygen getter just prior to the silicon evaporation. Pellets of titanium [15] were placed in a graphite crucible liner which occupied a second crucible pocket. Lumps of 99.95% pure ^{nat}Si obtained from Sigma-Aldrich occupied a tantalum crucible liner in the third crucible position. Initial tests with natural silicon utilized ~3 g of material in the crucible liner. To aid even deposition onto the substrate, the materials were melted prior to evaporation. To accomplish melting of the $BaCl_2$ and silicon, the e-beam was operated in low power mode, 2% (20 W) and 5% (50 W) respectively.

The $BaCl_2$ was evaporated on the substrate using an e-beam evaporator power of 3.5% to achieve a rate of ~300 Å/s until a total of 75 kÅ was deposited as measured by the QCM. Following $BaCl_2$ deposition, the shutter was moved into place and the titanium was heated using 20% beam power to getter residual oxygen. The shutter was subsequently removed and silicon was deposited onto the substrate at an e-beam evaporator power of 35%. Foils corresponding to a deposition of ~9.5 kÅ on the substrate were fabricated. This is a thickness of ~ 220 μg/cm^2. At 35% beam power the rate of deposition was ~10 Å/s. Approximately 85 mg of material was used during each evaporation.

Following vapor deposition, the heating block was kept at a temperature around 360 °C at a pressure $<1 \times 10^{-6}$ torr for 24 h to anneal the foil. This annealing process acts to reduce any stresses in the foils arising from the evaporation process. After the annealing process, the foil, substrate, and heating block were allowed to cool to 130 °C in vacuum before venting the chamber using argon gas. The substrate was then removed from the chamber and interior of the chamber was wiped clean using de-ionized water followed by ethanol.

Floating and mounting foils. The foils produced had a silver, metallic appearance indicative of metallic silicon. The foils were released from the substrate using standard floating techniques onto the surface of de-ionized water. Upon release into the water, the foils sank to the bottom of the floating container. Foils were carefully manipulated to the surface of the water using the mounting frames. Initial floating tests showed the foils curled tightly upon themselves making them unrecoverable. The annealing process previously described mediated the curling of the foils. The foils were lifted by hand from the surface of the water onto aluminum frames, (0.64 mm thick), with central holes either 10 or 15 mm in diameter. Foils fabricated on tungsten substrates dissolved immediately during the floating process resulting in no usable targets. In contrast, foils produced on copper substrates were able to be successfully floated and mounted onto the frames. We hypothesize that, despite electropolishing, the surface of the tungsten substrates was rougher than the copper substrates with a roughness comparable to the thickness of the foils deposited. Each copper substrate was able to provide foils onto a maximum of three frames. Fig. 3 shows the metallic appearance of the foils. After mounting on frames when viewed with a light behind the foils, some small pinholes are visible as evident in Fig. 3. Despite these pinholes, these foils have not exhibited any significant deterioration after being stored for several months in covered containers under ambient conditions. We are currently investigating long-term storage of these foils under either vacuum or an inert gas.

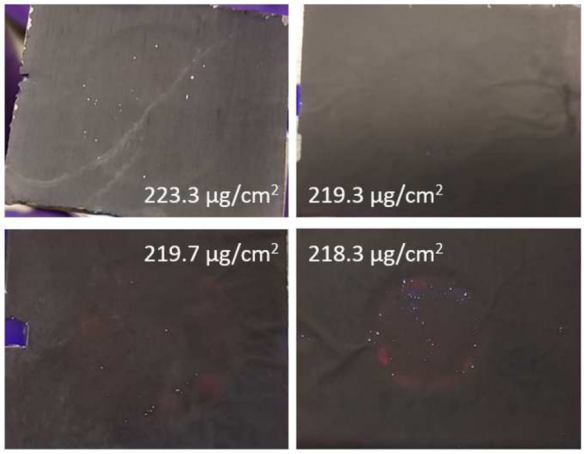

Fig. 3. Illumination of mounted silicon foils from below.

^{28}Si foil production. Following successful production of ^{nat}Si foils, the production of isotopically-enriched ^{28}Si foils was undertaken. Two grams of >99.8% ^{28}Si was obtained from the National Isotope Development Center at Oak Ridge National Lab. To utilize less ^{28}Si starting material, a custom tungsten crucible liner with smaller capacity was fabricated. Other than the use of this small-capacity crucible liner, the production of isotopically-enriched ^{28}Si foils followed the same procedure as described for making ^{nat}Si foils. Due to their success rate in the production of ^{nat}Si foils, copper substrates were used for the production of ^{28}Si foils. The procedure for floating and mounting the ^{28}Si foils onto frames was the same as ^{nat}Si foils.

4. Foil characterization

4.1. Foil thickness determination

Alpha particle energy loss measurement. Although the foil thickness was monitored during evaporation using the QCM, additional measurements were made to corroborate the QCM thickness values. The foil thickness was gauged by measuring the energy loss incurred for α particles of known energy traversing the foil. A spectroscopy-grade ^{148}Gd source (105 ± 1 nCi) was used to provide 3.183 MeV α particles for these measurements. Alpha particles from the source were collimated by a 1.15 cm diameter aperture before impinging on the foil. After passage through the foil the α particles were detected in a silicon surface barrier detector (SBD; Ortec TD-40-300-75) collimated to 0.635 cm diameter. After collimation the rate of α particles incident on the detector was ~20 counts/min. The energy of the α particle was measured with and without the intervening foil. The SBD was calibrated using a 1.0 μCi ^{226}Ra source. The 950 Å SBD dead layer was accounted for in the energy calibration. All energy loss calculations were done using SRIM-2013 TRIM calculations [16]. The energy loss through a 220 μg/cm^2 foil is ~160 keV. The uncertainty in the determination of the centroid of the α particle energy after traversing the foil is determined to be 2 keV (1.25%) which corresponds to a thickness uncertainty of 2.75 μg/cm^2. For the 13 foils for which both QCM and α

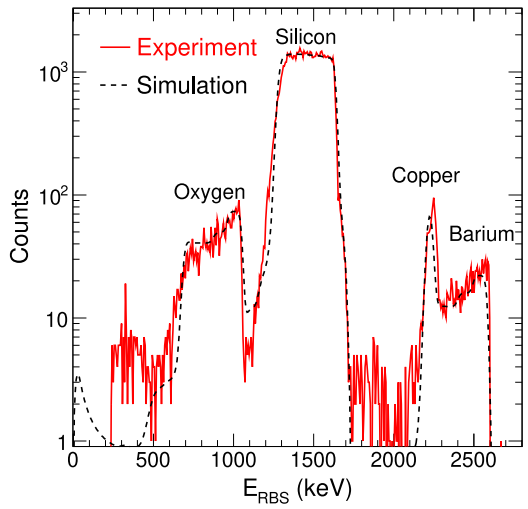

Fig. 4. RBS spectrum for a ^{nat}Si foil. The red, solid line corresponds to data while the black, dashed line corresponds to a simulated spectrum.

gauge measurements are available, the average thickness was measured to be 226.9 and 226.6 μg/cm^2, respectively. Foils originating from the same substrate exhibited a thickness variation between foils of up to ~10% with a systematic variation across the substrate observed. Note that the SRIM calculations did not account for any foil contaminants and, as such, provide an 'effective thickness' of Si. These values can be directly compared to those provided by the QCM as the QCM also does not account for foil contamination. The results of these measurements are presented in Table 1. The difference between the α-gauge and QCM measurements, $\Delta_{\alpha-QCM}$, is calculated as $\Delta_{\alpha-QCM} = ((\text{QCM} - \alpha)/\text{QCM}) * 100$. For the values measured, a maximum deviation of ±6.5% is observed. This relatively small variation suggests that the QCM provides a reasonable measure of the foil thickness during evaporation.

Rutherford backscattering measurements. Foil thickness can also be determined using Rutherford backscattering. RBS measurements were conducted at Hope College's 1.7 MV Pelletron particle accelerator using 2.905 MeV α particles. An experimental spectrum of the RBS data representative of the foils made in this work is shown in Fig. 4. The most prominent feature of the spectrum is a wide peak ranging from 1300–1700 keV which corresponds to scattering from silicon nuclei. At lower energies, 700–1000 keV, the peak arising from scattering with oxygen nuclei is observed. The asymmetry in this peak indicates a non-uniform distribution of the oxygen through the foil. A gaussian-like peak appears at 2200 keV with a plateau on the high-energy side that extends past 2500 keV. Residual copper diffusing from the substrate into the foil is responsible for the peak while barium from the release agent is responsible for the plateau. All but one of the RBS thicknesses given in Table 1 are in reasonable agreement with the QCM and α gauge values. The discrepant result for foil 23 is not presently understood.

4.2. Foil elemental abundance determination

Rutherford backscattering measurements. In addition to providing information on the foil thickness, RBS provides information on the elemental abundances of a foil. A simulated RBS spectrum created using SIMNRA software [17] is shown in Fig. 4 as a dashed curve superimposed on the RBS data. Simulated spectra account for variation in abundances through the foils by segmenting the foil into multiple layers of varying thicknesses and elemental abundances. The asymmetry of the oxygen peak in the RBS spectrum reveals an increased oxygen content at one surface of the foil. Analysis of the RBS data reveals that beyond this enhanced oxygen surface layer, in the bulk region of the foil, the silicon content is 90%–95%. The copper and barium peaks seen in the RBS spectra demonstrates that each of these elements constituted less than 1% of the total abundance in each foil. The silicon abundance for each foil was calculated as the average silicon content over all layers in the foil, including the enhanced oxygen surface layer. A summary of silicon content for measured foils is given in Table 2.

Table 1
Thickness of silicon foils as characterized by QCM, α gauge, and RBS measurements. All thicknesses are given in μg/cm^2. The quantity $\Delta_{\alpha-QCM}$ is expressed in percent.

Foil ID	Material	QCM	α	$\Delta_{\alpha-QCM}$	RBS
18	^{28}Si	218.8	–	–	–
19	^{28}Si	219.0	–	–	–
20	^{nat}Si	215.5	–	–	–
21	^{nat}Si	250.5	–	–	–
22	^{nat}Si	223.2	–	–	210
23	^{nat}Si	218.6	204.5	−6.5	299
24	^{nat}Si	218.3	223.9	2.6	–
25	^{nat}Si	217.4	228.9	5.3	–
26	^{nat}Si	218.0	221.2	1.5	–
27	^{nat}Si	219.4	220.8	0.6	–
29	^{nat}Si	219.3	205.5	−6.3	–
30	^{nat}Si	227.8	230.1	1.0	–
31	^{nat}Si	233.1	223.3	−4.2	–
32	^{nat}Si	292.6	285.5	−2.4	–
33	^{nat}Si	223.3	236.6	6.0	195
34	^{nat}Si	223.2	228.8	2.5	200
35	^{nat}Si	219.7	226.4	3.0	–
36	^{nat}Si	219.3	210.5	−4.0	–

Table 2
Assessment of silicon content using XPS and RBS.

Foil ID	Material	XPS %Si	RBS %Si
18	^{28}Si	88.5	–
20	^{nat}Si	87.3	–
22	^{nat}Si	–	87.57
23	^{nat}Si	–	89.44
27	^{nat}Si	89.6	–
33	^{nat}Si	90.4	89.34
34	^{nat}Si	86.8	89.75

X-ray photoelectron spectroscopy measurements. In order to provide an independent check of elemental abundances in the foil, X-ray photoelectron spectroscopy was used. XPS measurements were taken using a PHI VersaProbe II X-ray Microprobe system in the Indiana University Nanoscale Characterization Facility. The instrument allowed for sputtering of argon ions onto samples thus providing elemental analysis as a function of depth. The effective depth is based upon the rate of ion sputtering and the thickness determination from the QCM and α gauge measurements. At the surface of the foil, the argon ion is sputtered using 1 kV accelerating potential while in the bulk the accelerating potential is increased to 4 kV. As the ion sputtering rate is varied between the foil surface and the bulk, an uncertainty exists in the relative depth between these two regions. In assessing the elemental abundance in the bulk of the material the sputtering rate is held constant. A representative foil depth profile is presented in Fig. 5. A silicon oxide layer is clearly observed on the front side of the foil which contains a much higher oxygen content than the bulk foil, in qualitative agreement with the RBS results. This oxide layer extends for approximately 100 nm inside the foil. The thickness of this oxide layer is significantly larger than the 1 nm thick oxide layer that typically forms as a result of room temperature oxidation [18]. This implies that the oxygen content in the foils produced originates prior to or during their production. Beneath this layer of silicon oxide the film appears relatively uniform with a silicon abundance of 85%–90%. The decrease in silicon abundance occuring around ~0.95 μm corresponds to the back side of the foil. The spike in carbon abundance at this depth is a background due to the mounting of the foil inside the XPS instrument. The carbon seen at the front of the foil is environmental carbon on the surface of the sample and is often observed in XPS measurements.

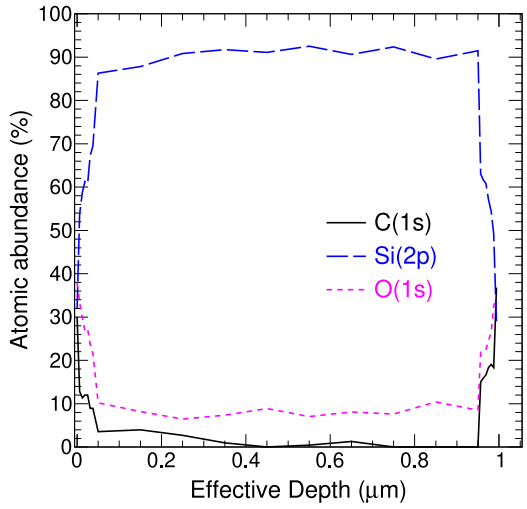

Fig. 5. XPS depth profile for various elements in a ^{nat}Si foil. The effective depth is based upon the ion accelerating voltage and the depth determination from the QCM and α gauge measurements.

The silicon abundances reported in Table 2 were calculated as the average abundance through the bulk foil, excluding the enhanced oxygen surface layers. The uncertainty in the relative depth between the surface and bulk layers prevents determination of the elemental abundance over the entire foil. Both the RBS and XPS measurements demonstrate the ability to produce silicon foils with silicon purity of 87%–90%. The RBS and XPS results for foils 33 and 34 shows that the determination of the silicon content is consistent within 3%.

5. Conclusion

Both ^{nat}Si and ^{28}Si foils with a thickness of ~220 μg/cm^2 and a low oxygen content were produced via vapor deposition. The foils have a silvery, metallic color and do not exhibit any visible signs of deterioration even after several months of storage under ambient conditions. The thickness of the foils was characterized using measurements from both a QCM and ^{148}Gd α particle gauge. These measurements were in agreement to within <0.5% on average, which indicated that the QCM could be used as a reliable measure of the foil thickness during evaporation. In general, RBS thickness measurements were qualitatively consistent with the determined thicknesses. Measurements of elemental abundances using XPS and RBS showed silicon purity to be 87%–90% with the primary contaminant being oxygen. An enhanced oxygen content of up to 40% was observed at the foil surface. These foils manifest an approximately 4-fold reduction in the oxygen content as compared to previous foils. This reduced oxygen content reduces a significant source of background thus improving future fusion cross-section measurements.

Declaration of competing interest

The authors declare that they have no known competing financial interests or personal relationships that could have appeared to influence the work reported in this paper.

CRediT authorship contribution statement

J.E. Johnstone: Investigation, Formal analysis. **S. Hudan:** Investigation. **C. Folluo:** Methodology. **T. Werke:** Methodology. **P.A. DeYoung:** Investigation. **R.T. deSouza:** Supervision, Writing - original draft, Writing - review & editing.

Acknowledgments

The isotope(s) used in this research was supplied by the Isotope Program within the Office of Nuclear Physics in the Department of Energy's Office of Science. Access to XPS at the Nanoscale Characterization Facility was provided by the National Science Foundation, USA Award DMR MRI-1126394. The authors gratefully acknowledge the support of the Mechanical Instrument Services facility at Indiana University, USA. This work was supported by US Department of Energy under Grant No. DE-FG02-88ER-40404 (Indiana University) and National Science Foundation, USA award PHY-1613188 (Hope College).

References

[1] 2015 NSAC Long Range Plan: The Frontiers of Nuclear Science, http://science.energy.gov/np/nsac/.
[2] J. Vadas, et al., Phys. Rev. C 97 (2018) 031601(R).
[3] A.M. Sandorfi, et al., Nucl. Instrum. Methods 136 (1976) 395–396.
[4] A.J. Michielsen, P. Decowski, Nucl. Instrum. Methods A A282 (1989) 121–123.
[5] Vendor for water chiller (WW2), Haskris, 2019, URL https://haskris.com.
[6] Vendor for turbomolecular and scroll pump (STP-603), Edwards, 2019, URL https://www.edwardsvacuum.com/en.
[7] Vendor for cryopump (CTI-8), PTB sales, 2019, URL www.ptbsales.com.
[8] Vendor for RGA (RGA 200), Stanford research systems, 2019, URL https://www.thinksrs.com/index.html.
[9] Vendor for linear motion feedthrough (L-2212-6), Huntington vacuum products, 2019, URL https://huntvac.com/.
[10] Vendor for quartz crystal monitor, Model 851, Telemark, 2019, URL https://telemark.com/.
[11] Vendor for tantalum wire, Goodfellow, 2019, URL www.goodfellowusa.com.
[12] John R. Rumble Jr. (Ed.), CRC Handbook of Chemistry and Physics, hundredth ed., CRC Press/Taylor and Francis, Boca Raton, FL, 2019.
[13] B.-F. Ju, Y.-L. Chen, M. Fu, Y. Chen, Y. Yang, Sensors Actuators A 155 (2009) 136–144.
[14] A.M. Awad, N.A.A. Ghany, T.M. Dahy, Appl. Surf. Sci. 256 (2010) 4370–4375.
[15] Vendor for titanium pellets, Kurt J. Lesker, 2019, URL https://www.lesker.com.
[16] Stopping and range of ions in matter, SRIM, 2019, URL www.srim.org.
[17] M. Mayer, SIMNRA User's Guide, Report IPP 9/113, Max-Planck-Institut fur Plasmaphysik, Garching, Germany, 1997.
[18] L. Filipovic, Topography Simulation of Novel Processing Techniques, Vol. E360 (Ph.D. thesis), 2012, URL http://www.iue.tuwien.ac.at/phd/filipovic/.